Brain Imaging and Behavior (2019) 13:220–231
https://doi.org/10.1007/s11682-018-9842-z

ORIGINAL RESEARCH

Quantitative susceptibility mapping as a biomarker for evaluating white matter alterations in Parkinson's disease

Xiaojun Guan[1] · Peiyu Huang[1] · Qiaoling Zeng[1] · Chunlei Liu[2,3] · Hongjiang Wei[2] · Min Xuan[1] · Quanquan Gu[1] · Xiaojun Xu[1] · Nian Wang[4] · Xinfeng Yu[1] · Xiao Luo[1] · Minming Zhang[1]

Published online: 7 February 2018

Abstract

Myelinated white matter showing diamagnetic susceptibility is important for information transfer in the brain. In Parkinson's disease (PD), the white matter is also suffering degenerative alterations. Quantitative susceptibility mapping (QSM) is a novel technique for noninvasive assessment of regional white matter ultrastructure, and provides different information of white matter in addition to standard diffusion tensor imaging (DTI). In this study, we used QSM to detect spatial white matter alterations in PD patients (n = 65) and age- and sex-matched normal controls (n = 46). Voxel-wise tract-based spatial statistics were performed to analyze QSM and DTI data. QSM showed extensive white matter involvement—including regions adjacent to the frontal, parietal, and temporal lobes—in PD patients, which was more widespread than that observed using DTI. Both QSM and DTI showed similar alterations in the left inferior longitudinal fasciculus and right cerebellar hemisphere. Further, alterations in the white matter were correlated with motor impairment and global disease severity in PD patients. We suggest that QSM may provide a novel approach for detecting white matter alterations and underlying network disruptions in PD. Further, the combination of QSM and DTI would provide a more complete evaluation of the diseased brain by analyzing different biological tissue properties.

Keywords Parkinson's disease · White matter · Quantitative susceptibility mapping · Biomarker

Introduction

Parkinson' disease (PD) is a progressive neurodegenerative disorder that causes extensive pathological alterations throughout the brain. According to the Braak staging scheme for PD, the primary pathology occurs in the brainstem and then progressively ascends through the brain to ultimately reach the neocortex (Braak et al. 2003, 2004). The myelinated white matter fibers in the brain, which form a complex network to connect and relay information between different grey matter regions, can also exhibit degenerative alterations in PD.

Diffusion tensor imaging (DTI) is the most common tool for assessing the structural integrity of white matter tracts in PD brain. To date, DTI findings consistently showed widespread abnormalities in PD patients with cognitive impairment (Gallagher et al. 2013; Kamagata et al. 2013; Agosta et al. 2014; Auning et al. 2014) while the results were conflicting in the studies of non-demented PD patients (Surdhar et al. 2012; Kamagata et al. 2013; Agosta et al. 2014; Worker et al. 2014; Chen et al. 2015). Though it is to say that DTI could be used to quantify white matter myelination (Song et al. 2002), limitations exist. Signals from DTI are influenced by numerous physiological processes including underlying fiber organization, extracellular space, axon diameter, and membrane permeability (Beaulieu 2002; Neil

Xiaojun Guan and Peiyu Huang contribute equally to this paper.

Electronic supplementary material The online version of this article (https://doi.org/10.1007/s11682-018-9842-z) contains supplementary material, which is available to authorized users.

✉ Minming Zhang
zhangminming@zju.edu.cn

1 Department of Radiology, The Second Affiliated Hospital, Zhejiang University School of Medicine, Hangzhou, China

2 Department of Electrical Engineering and Computer Sciences, University of California, Berkeley, CA, USA

3 Helen Wills Neuroscience Institute, University of California, Berkeley, CA, USA

4 Brain Imaging and Analysis Center, Duke University School of Medicine, Durham, NC, USA

et al. 2002; Jones et al. 2013). Thus, DTI changes in the white matter cannot be solely attributed to changes in myelination (Argyridis et al. 2013; Jones et al. 2013). Indeed, a recent histological study reported no significant correlation between DTI changes and myelination (Argyridis et al. 2013). Thus, new techniques are required to provide further information on white matter alterations in PD.

The myelin sheath is the predominant source of susceptibility contrast in the deep white matter, mainly because of its diamagnetic property, which differs according to the complexity of white matter fiber organization (Liu et al. 2011, 2015; Li et al. 2012; Lodygensky et al. 2012). It is well established that quantifying the susceptibility of white matter can be used to assess the trajectory of white matter development (Lodygensky et al. 2012; Argyridis et al. 2013; Li et al. 2014). Quantitative susceptibility mapping (QSM) is a novel contrast technique for quantification of magnetic susceptibility, which involves deconvolution of the influence of neighboring voxels on changes in the magnetic field (Liu et al. 2011; Li et al. 2012, 2014; Argyridis et al. 2013; Li and Liu 2013). QSM has been used to show nigral iron deposition in PD patients (Du et al. 2015; He et al. 2015; Murakami et al. 2015; Guan et al. 2017a). In contrast to paramagnetic iron, myelinated white matter tracts show a low susceptibility value resulting from the diamagnetic property of myelin, while demyelination is associated with increased susceptibility. Previously, QSM has been widely used to investigate the pathologic changes of white matter during the progression of multiple sclerosis (Rudko et al. 2014). Given this relationship between magnetic susceptibility and myelin content (Argyridis et al. 2013), QSM may be useful endogenous biomarker for assessing the intensity of myelination in PD (Liu et al. 2011; Li et al. 2012; Argyridis et al. 2013; Li and Liu 2013).

In the present study, we used QSM to examine the alterations in white matter ultrastructure (by quantifying susceptibility) in a cohort of PD patients and age- and sex-matched healthy control subjects, and compared these findings with typical DTI variables, including fractional anisotropy (FA), mean diffusivity (MD), axial diffusivity (AD) and radial diffusivity (RD) (Song et al. 2002; Auning et al. 2014). We hypothesized that QSM would provide novel ultrastructural data on white matter alterations in PD, and, to some extent, QSM and DTI would provide similar disease information in certain white matter.

Methods

Subjects

Informed consent was provided by each subject in the study. The methods were performed in accordance with the approved guideline and regulation, and experimental protocols were approved by the Medical Ethic Committee of the Second Affiliated Hospital of Zhejiang University School of Medicine. Control subjects and PD patients with a history of neurologic or psychiatric disorders (e.g. infarction or encephalatrophy), brain trauma, or general exclusion criteria for MR scanning (e.g., metal implants) were excluded from this study. One hundred and twenty-two subjects including 73 PD patients diagnosed by an experienced neurologist according to the United Kingdom Brain Bank criteria (Hughes et al. 1992) and 49 normal controls were initially included.

The subscales of the Unified Parkinson's Disease Rating Scale (UPDRS), disease duration, and the Mini-Mental State Examination (MMSE) scores were recorded for all patients immediately after MR scanning. According to MMSE estimated by the criteria suitable for Chinese population (Katzman et al. 1988; Zhang et al. 1990) (MMSE score ≤ 17 for illiterate subjects, ≤ 20 for grade-school literate, and ≤ 23 for junior high school and higher education literate), all our recruited patients were non-demented. Before clinical assessments and MR scanning, PD patients who were under medication terminated anti-parkinsonian medication for at least 12 h. Demographic data of control subjects and PD patients are shown in Table 1.

Scanning protocols

A three-dimensional (3D) multi-echo gradient-echo (GRE) pulse sequence (termed enhanced T2 star-weighted angiography [ESWAN]), Fluid-attenuated inversion recovery

Table 1 Group demographics and clinical status

	Normal controls	Patients	*p* values
Number	46	65	–
Sex (male/female)	21/25	32/33	0.847
Age, y, mean ± SD	57.8 ± 9.4	55.5 ± 9.5	0.211
Disease duration, y, mean ± SD	–	4.7 ± 3.9	–
H-Y stages,mean ± SD	–	2.3 ± 0.7	–
MMSE,mean ± SD	–	27.8 ± 2.2	–
UPDRS I scores, mean ± SD	–	1.9 ± 2.6	–
UPDRS II scores, mean ± SD	–	9.6 ± 5.4	–
UPDRS III scores, mean ± SD	–	27.1 ± 14.4	–
Score from right side	–	10.0 ± 5.7	–
Score from left side	–	9.31 ± 6.6	–
UPDRS total scores, mean ± SD	–	40.5 ± 21.7	–
Head rotation angle, mean ± SD	12.2 ± 5.6	13.4 ± 5.7	0.256

(FLAIR), DTI, and 3D T1-weighted images were acquired on a 3.0-T MR scanner using an 8-channel head coil (Signa Excite; GE Medical Systems, Milwaukee, WI, USA). During scanning, the head of each participant was stabilized with restraining foam pads, and earplugs were provided to reduce noise. Data would be discarded or rescanned if head motion appeared. The 3D-GRE ESWAN parameters with a right/left frequency encoding direction achieved in the continuous axial plane were: TR = 45 ms, echo numbers = 8, TE_1/spacing/TE_8 = 5/5.02/40.14 ms, flip angle = 25°, matrix size = 240 × 240, slice thickness = 2.8 mm, FOV = 200 × 200 mm, reconstructed in-plane resolution = 0.78125 × 0.78125, slices = 52, ASSET = 2, and no gap. DTI data were acquired using a GRE-echo-planar imaging sequence (GRE-EPI) with 15 noncollinear diffusion-sensitization gradients (b = 1000s/mm^2) in the continuous axial plane using the following parameters: TR = 10 s, TE = 86 ms, FOV = 240 × 240 mm, matrix size = 128 × 128, flip angle = 90°, slice thickness = 3 mm, slice = 38, and no gap. To calculate the fiber angle in all subjects, 3D T1-weighted images were acquired in the sagittal plane using the following parameters: TR = 5100 ms, TE = 1.2 ms, FOV = 240 × 240 mm, matrix size = 256 × 256, flip angle = 15°, slice thickness = 1.2 mm, slice = 124, and no gap. FLAIR images were also used to semi-quantify the white matter hyperintensity (WMH), the parameters were: TR = 9602 ms, TE = 146 ms, FOV = 240 × 240 mm, matrix size = 512 × 512, flip angel = 90°, slice thickness = 5 mm, slice = 23. Of note, due to FLAIR data from one controls and four patients were lost, a total of 106 subjects were included in WMH scaling. These four modalities were obtained sequence-by-sequence in each subject. The total scanning time was approximately 14 min.

QSM reconstruction

QSM reconstruction was performed as previously reported (Li et al. 2014; Guan et al. 2017b). A computer cluster running susceptibility imaging software (STI suite; https://people.eecs.berkeley.edu/~chunlei.liu/software.html) was used to process the phase images. Phase images of ESWAN sequence were unwrapped using a Laplacian-based phase unwrapping method (Li et al. 2011, 2015). The unwrapped phase images from all coils were normalized by the corresponding echo times and averaged to determine the frequency shift, which was used to remove the background frequency by the V-SHARP method (with a spherical mean radius increasing from 0.6 mm at the boundary of the brain to 25 mm toward the center of the brain) (Wu et al. 2012; Li et al. 2014). By using the susceptibility of cerebrospinal fluid as a reference, QSM images were derived by computing the resulting tissue phase using an improved sparse linear equation and least-squares algorithm (Li et al. 2015) (Fig. 1).

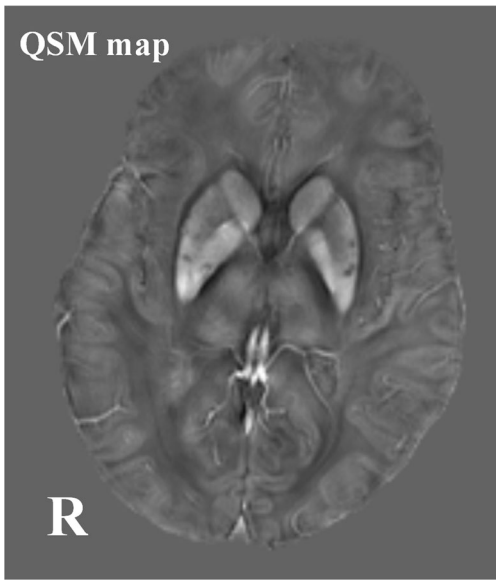

Fig. 1 Raw QSM map processed by susceptibility imaging software (STI suite; University of California, Berkeley, CA, USA)

The measurement of QSM is influenced by fiber orientation in the magnetic field. Although most people have similar brain fiber structures, differences in the head position in the scanner between subjects can result in differences in fiber orientation. Thus, we calculated the head rotation angle (HRA) relative to the B0 field (Li et al. 2012). HRA values were calculated using three steps: (1) structural images were coregistered to the ESWAN images; (2) the coregistered structural images were normalized into standard space; and (3) HRA values were then calculated using the transformation matrix from step 2.

Tract-based spatial statistics processing

Diffusion-weighted images were analyzed using a brain fMRI software library (FSL, v4.1.0; http://www.fmrib.ox.ac.uk/fsl). First, the original data were converted to compressed FSL NIFTI format, and then skull stripping was performed using the brain extraction toolbox. After eddy current correction, diffusion tensors were reconstructed and the diffusion parameters were calculated. The resulting FA images were further processed using tract-based spatial statistics, which performs voxel-by-voxel whole-brain analysis. After aligning all individual FA images to the Montreal Neurological Institute (MNI) standard space template using nonlinear registration, the mean FA image was calculated and compressed to form a mean skeleton representing the topological features of all tracts derived from the whole group. An FA threshold of 0.3 was set to remove trivial tracts. Then, each subject's aligned FA images were projected onto the fiber skeleton template for statistical

analyses. Meanwhile, QSM maps were coregistered with DTI images through raw ESWAN images. We calculated the other parameters like MD, AD and RD as well, especially the RD maps for it was reported to be closely correlated with myelination (Song et al. 2002). Finally, MD, AD, RD, and QSM maps were normalized to the skeleton using tract-based spatial statistics. Given that poor image quality mainly resulting from motion artifact would lead to coregistration failure, QSM and DTI data from 11 subjects including eight PD patients and three normal controls were discarded. Finally, PD patients (32 men, 33 women) with a mean age of 55.5 ± 9.5 years and healthy control subjects (21 men, 25 women) with a mean age of 57.8 ± 9.4 years were included in the further statistics analysis.

Statistics analysis

To perform demographic comparisons between PD patients and healthy controls, we used independent t-test for age and Pearson Chi square for sex. The scores of periventricular WMH (PWMH) and deep WMH (DWMH) assessed according to a widely used specialized scale (Fazekas et al. 1987) were compared between PD patients and controls by using Fisher exact test (details in supplementary materials Table 1S and 2S).

DTI data were analyzed using independent two sample t-test with the FSL randomize procedure with 5,000 permutations. Although there was no difference in age and sex between the groups, they were considered as covariates to avoid any interference. In addition, to minimize the influence of HRA on the mean magnetic susceptibility (MMS) (Lee et al. 2010; Li et al. 2012), HRA was added as an extra covariate. Correction for multiple comparisons was performed using a cluster-based thresholding method ($p < 0.001$, continuous cluster size > 10). The clusters from QSM and DTI data survived by above threshold would be extracted and overlapped in the MNI space to observe whether these two modalities could detect similar disease information in the present study.

To assess whether clinical features were associated with white matter regions exhibiting significant differences in tissue susceptibility and DTI variables, the average regional values were extracted to perform correlation analyses. A partial Pearson correlation analysis was performed between clinical features and imaging indices. For analysis of DTI variables, age and sex were included as covariates. For analysis of QSM, age, sex and HRA values were included as covariates. Complementary, for PD is an asymmetric disease with laterization, we also did correlation analyses between the motor impairment from each side and the correspondingly contralateral white matter regions. $P < 0.05$ was considered statistically significant (without multiple comparison correction as an explorative study). Statistical analyses were performed with statistical software (IBM SPSS Statistics v19.0; IBM Co., Armonk, NY, USA).

Results

Demographic and clinical features and WMH distribution

PD patients were well matched to the healthy control subjects for age ($p = 0.211$) and sex ($p = 0.700$). Further, there was no difference in the HRA between the groups. Group demographics and clinical status data are shown in Table 1. No significant difference was observed in PWMH (p = 0.079) and DWMH (p = 0.599) between two groups (details in supplementary materials Table 1S and 2S).

White matter alterations in PD patients

QSM showed widespread involvement of the white matter, including increased MMS, in PD patients compared with control subjects (Fig. 2, QSM). The affected white matter regions covered the frontal, parietal, and temporal lobes, including the bilateral external capsule (EC), inferior longitudinal fasciculus (ILF), inferior fronto-occipital fasciculus, left superior longitudinal fasciculus (SLF), right anterior thalamic radiation, left cingulum (cingulate gyrus; Cg) and the body of the corpus callosum. In contrast, regions with decreased MMS included the bilateral deep white matter of the frontal lobes and the right cerebellar hemisphere. There were no differences in other white matter regions between the groups.

PD patients showed a significant reduction in FA only in the right uncinated fasciculus (UF) compared with healthy controls (Fig. 2, FA), while there was a significant increase in MD in the right EC and forceps minor, and in the left cingulum (hippocampus; Ch) (Fig. 2, MD). In addition, there was a significant increase in RD in the left Ch, left ILF, and right SLF (Fig. 2, RD) and decrease in AD in the left Ch and right ILF (Fig. 2, AD). We also observed a region of decreased RD in the right cerebellar hemisphere. These data were shown in Table 2 in detail. There were no regions of increased FA or AD or decreased MD between PD patients and healthy controls.

Overlaps of white matter alterations between QSM and DTI

Although QSM and DTI describe different biophysical properties of the white matter, they can both be used to assess white matter myelination. Thus, we performed a cross-validation of white matter alterations observed with QSM and DTI. Both QSM and DTI showed an increase in MMS and

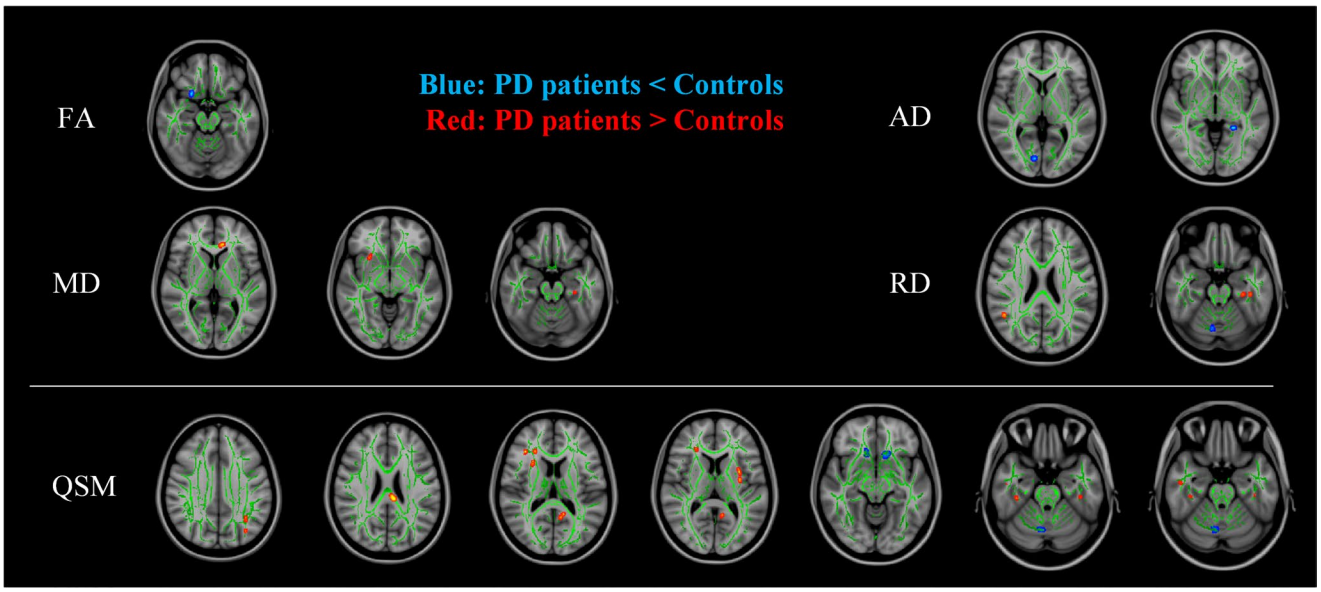

Fig. 2 Intergroup differences of quantitative susceptibility mapping (QSM) and diffusion tensor imaging (DTI) variables ($p < 0.001$, cluster size > 10). Results are shown overlaid on an MNI152 template and the mean fractional anisotropy (FA) skeleton (green)

RD in the left ILF, and a decrease in MMS and RD in the right cerebellar white matter (Figs. 3 and 4). There were no other regions of overlap between the two modalities.

Clinical relevance of regional white matter alterations

Using QSM data, we assessed the clinical significance of regional white matter changes in PD patients (Fig. 5). In the right ILF, there was a significant correlation of increased MMS with UPDRS total score (r = 0.314, $p = 0.013$). In the right Cg, there was a significant correlation of increased MMS with disease duration (r = 0.282, $p = 0.026$). Oppositely, there were also weak negative correlations of decreased MMS in the left deep white matter of the frontal lobe with motor score from right side of limbs (r = -0.300, p = 0.015, uncontrolled), UPDRS II score (r = − 0.285, $p = 0.021$, uncontrolled) and disease duration (r = − 0.265, $p = 0.033$, uncontrolled) while the only correlation with lateralized motor score was survived after controlling for age, HRA and sex (r = -0.259, p = 0.042), suggesting a trend of increase in myelin content with disease progression.

For DTI, there were significant correlations of increased RD and MD in the Ch with disease severity including UPDRS III score (r = 0.328, $p = 0.009$; r = 0.3861, $p = 0.002$, respectively) and UPDRS total score (r = 0.327, $p = 0.009$; r = 0.378, $p = 0.002$, respectively). In addition, significant correlation between MD in the Ch and UPDRS II (r = 0.303, $p = 0.016$) was observed. All analyses were controlled for age and sex. RD and MD data were shown in Fig. 6.

No other correlation was observed in our PD cohort.

Discussion

In the present study, we describe the first use of QSM for *in vivo* imaging of the brain white matter in PD patients, and provide a comparison of the underlying white matter alterations as assessed by QSM and DTI. A major finding was that QSM was able to detect extensive white matter alterations in PD patients, which occurred predominantly in regions adjacent to the frontal, parietal, and temporal lobes. Further, both QSM and DTI showed similar white matter alterations in the right cerebellar hemisphere and the left temporal lobe. Finally, regional changes in white matter MMS, RD, and MD were significantly correlated with disease severity and disease duration.

PD patients are known to develop white matter degeneration. In the present study, QSM demonstrated a spatially extensive involvement of the white matter adjacent to the frontal, parietal, and temporal lobes, the EC, body of the corpus callosum, and the Cg. Normal myelin shows a low MMS because of its diamagnetic properties (Liu et al. 2011, 2015; Li et al. 2012; Lodygensky et al. 2012), and MMS also differs according to the complexity of white matter fiber organization. Thus, in the present study, the increase in MMS may reflect damage to the white matter and a reduction in myelin content, which was demonstrated that MMS is only minimally influenced by white matter iron content (Lodygensky et al. 2012).

We also observed changes in DTI parameters in the white matter of PD patients, including the UF, SLF, EC, forceps minor, Ch, and ILF, as previously reported (Karagulle et al. 2008; Gattellaro et al. 2009; Rae et al. 2012; Zhan et al.

Table 2 Differences of white matter alterations between Parkinson's disease and healthy controls

Comparisons	Maps	Brain regions	L/R	Cluster size	MNI coordinate			Parkinson's disease (m^2/s or ppm)	Healthy controls	*p* value
					X	Y	Z			
Patients < controls	FA	Uncinate fasciculus	R	14	22	12	-18	0.2801 ± 0.0442	0.3231 ± 0.0645	< 0.001
Patients > controls	MD	Forceps minor	-	42	-9	33	2	0.000080 ± 0.00007	0.00073 ± 0.00010	< 0.001
	MD	External capsule	R	14	27	16	-6	0.00082 ± 0.00007	0.00077 ± 0.00007	< 0.001
	MD	Cingulum (hippocampus)	L	10	-31	-25	-19	0.00085 ± 0.00008	0.00078 ± 0.00007	< 0.001
Patients < controls	AD	Inferior longitudinal fasciculus	R	20	10	-80	4	0.00116 ± 0.00015	0.00130 ± 0.00021	< 0.001
	AD	Cingulum(hippocampus)	L	13	-23	-43	-3	0.00090 ± 0.00008	0.00097 ± 0.00010	< 0.001
Patients < controls	RD	Cerebellum**	R	14	9	-68	-24	0.00057 ± 0.00007	0.00066 ± 0.00016	< 0.001
Patients > controls	RD	Cingulum (hippocampus)	L	14	-29	-27	-19	0.00066 ± 0.00008	0.00061 ± 0.00006	< 0.001
	RD	Superior longitudinal fasciculus	R	13	48	-51	22	0.00074 ± 0.00017	0.00064 ± 0.00009	< 0.001
	RD	Inferior longitudinal fasciculus*	L	10	-39	-27	-25	0.00064 ± 0.00008	0.00058 ± 0.00005	< 0.001
Patients < controls	MMS	Frontal deep white matter	L	93	-8	18	-17	-0.0239 ± 0.0169	-0.0105 ± 0.0130	< 0.001
	MMS	Cerebellum**	R	56	7	-66	-26	-0.0206 ± 0.0105	0.0126 ± 0.0124	< 0.001
	MMS	Frontal deep white matter	R	23	13	26	-10	-0.0206 ± 0.0149	-0.0096 ± 0.0136	< 0.001
Patients > controls	MMS	Body of corpus callosum	-	37	-7	-29	23	0.0000 ± 0.0128	-0.0078 ± 0.0101	0.001
	MMS	Cingulum (cingulate gyrus)	L	36	-10	-54	9	0.0187 ± 0.0146	0.0081 ± 0.0126	< 0.001
	MMS	External capsule	L	35	-32	1	6	-0.0129 ± 0.0161	-0.0214 ± 0.0104	0.003
	MMS	Anterior thalamic radiation	R	25	25	29	15	-0.0118 ± 0.0075	-0.0176 ± 0.0065	< 0.001
	MMS	External capsule	R	19	27	12	16	-0.0230 ± 0.0092	-0.0287 ± 0.0097	0.004
	MMS	Inferior fronto-ocipital fasciculus	R	19	38	31	12	0.0073 ± 0.0081	0.0033 ± 0.0063	0.004
	MMS	Cingulum (cingulate gyrus)	L	17	-12	-50	18	0.0099 ± 0.0119	0.0022 ± 0.0107	< 0.001
	MMS	External capsule	L	17	-32	-7	7	0.0026 ± 0.0206	0.0072 ± 0.0114	0.006
	MMS	Inferior longitudinal fasciculus	R	14	38	-30	-29	-0.0168 ± 0.0179	-0.0338 ± 0.0165	< 0.001
	MMS	Superior longitudinal fasciculus	L	11	-34	-57	32	-0.0007 ± 0.0078	-0.0046 ± 0.0065	0.011
	MMS	Superior longitudinal fasciculus	L	11	-34	-73	34	0.0035 ± 0.0087	-0.0018 ± 0.0091	0.001
	MMS	Inferior longitudinal fasciculus	R	11	51	-11	-23	0.0002 ± 0.0132	-0.0095 ± 0.0154	< 0.001
	MMS	Inferior longitudinal fasciculus*	L	10	-39	-30	-27	-0.0228 ± 0.0228	-0.0373 ± 0.0204	0.003

Correction for multiple comparisons was performed using a cluster-based thresholding method ($p < 0.001$, continuous cluster size > 10). * or ** indicated the overlaps between the findings of DTI and QSM. FA, fractional anisotropy; MD, mean diffusivity; AD, axial diffusivity; RD, radial diffusivity; MMS, mean magnetic susceptibility; L, left; R, right; MNI, Montreal Neuroscience Institute template

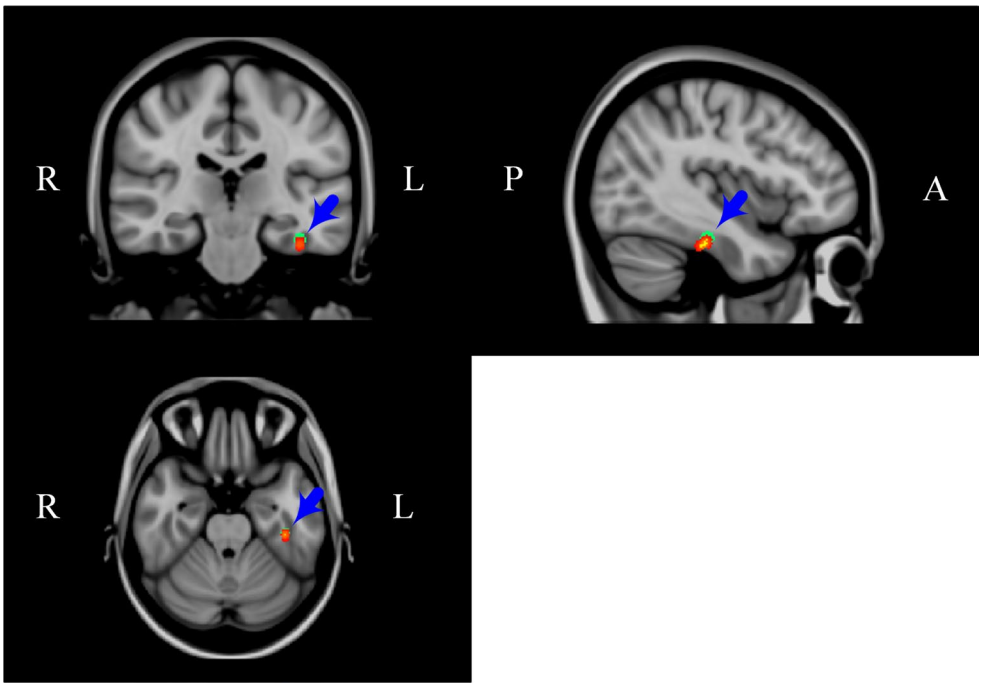

Fig. 3 Region of increased mean magnetic susceptibility (MMS) and radial diffusivity (RD) (red color, increased MMS; green color, increased RD) ($p < 0.001$, cluster size > 10). Results are shown overlaid on an MNI152 template

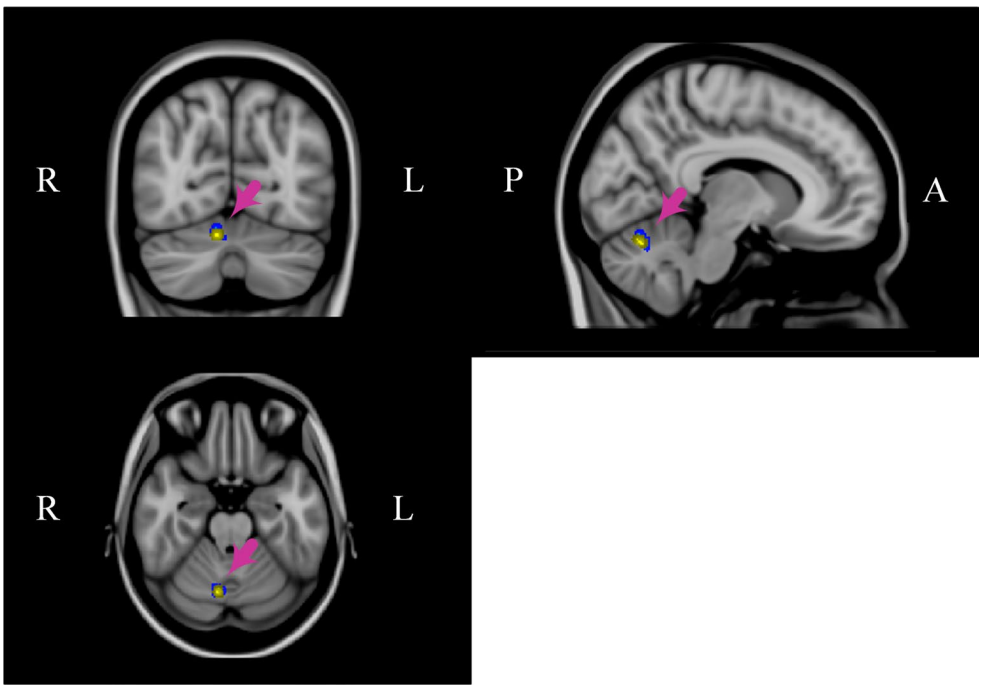

Fig. 4 Region of mean magnetic susceptibility (MMS) and radial diffusivity (RD) (blue, decreased MMS; yellow, decreased RD) ($p < 0.001$, cluster size > 10). Results are shown overlaid on an MNI152 template

2012; Agosta et al. 2013; Gallagher et al. 2013; Auning et al. 2014). However, DTI is unable to characterize diffusion in more than one direction in each image voxel, which reduces its sensitivity, particularly in regions of complicated white matter organization adjacent to the frontal lobe (Tuch et al. 2002; Jeurissen et al. 2013). Using QSM, however, we detected changes in this white matter region in PD patients. DTI data are also strongly affected by the extracellular space, axonal diameter, and membrane permeability (Beaulieu 2002; Neil et al. 2002; Jones et al. 2013). Thus, our data suggest that QSM can improve the detection of regional ultrastructural changes in the white matter of PD patients.

Although QSM and DTI data reflect completely different biophysical properties, we found similar changes in MMS and RD using these techniques. For example, both QSM and DTI showed decreased MMS and RD in the right cerebellar hemisphere, and increased MMS and RD in the

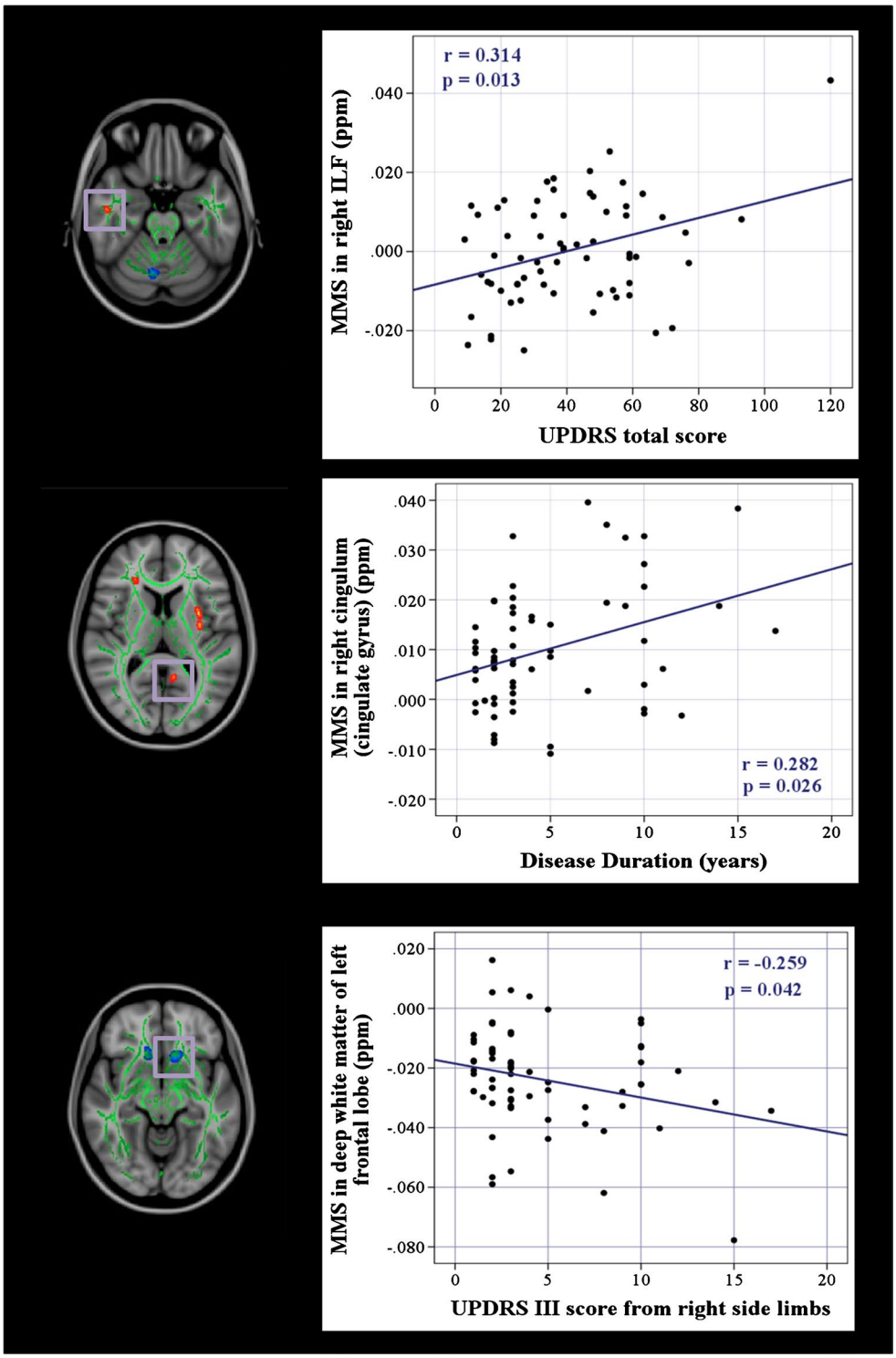

Fig. 5 Clinical correlations of regional mean magnetic susceptibility (MMS). Age, sex and head rotation angle (HRA) value were regarded as covariates

left temporal lobe, in patients with PD. Both MMS and RD can detect the integrity of the myelin sheath, although they reflect different tissue properties. MMS quantifies the susceptibility contrast of myelin (Liu et al. 2011, 2015; Li et al. 2012; Lodygensky et al. 2012), while RD from DTI reflects the diffusivity of water molecules perpendicular to axonal fiber tracts (Song et al. 2002). These results suggest that QSM and DTI may provide similar findings in certain white matter regions in the same cohort of patients. Thus, previous DTI studies with negative findings in patients with PD (Surdhar et al. 2012; Kamagata et al. 2013; Agosta et al. 2014; Worker et al. 2014; Chen et al. 2015) could consider adding QSM for more complete assessment of white matter involvement in PD.

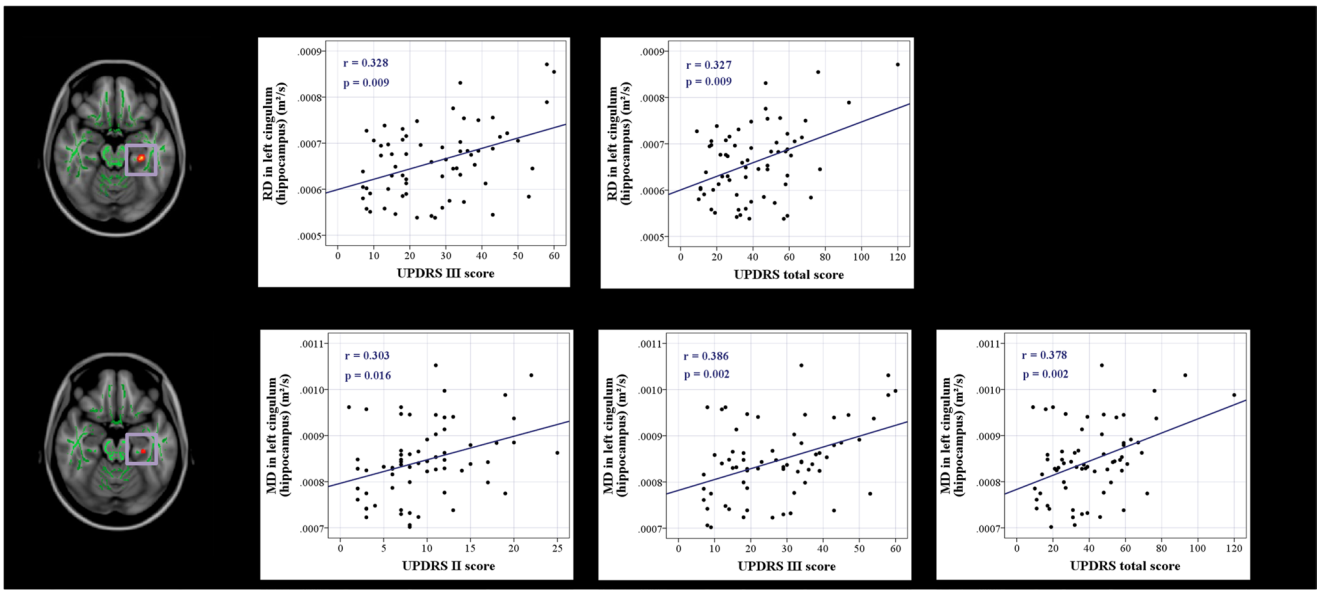

Fig. 6 Clinical correlations of regional radial diffusivity (RD) and mean diffusivity (MD). Age and sex were regarded as covariates

We also examined the clinical relevance of regional white matter alterations measured with MMS and DTI variables in patients with PD, and found significant positive correlations of MMS in the ILF with UPDRS total score (global disease severity), and of MMS in the Cg with disease duration. Using DTI data, we also observed significantly positive correlations of increased MD and RD in the Ch with disease severity. Taken together, our QSM and DTI data demonstrated involvement of the ILF and Ch contributed to motor impairment and global disease severity in PD. With disease progression, the Cg, a part of posterior cingulum that is highly related to cognitive function (Delano-Wood et al. 2012), showed a continued decrease in myelin integrity on QSM, although our patients showing normal clinical cognition. Nevertheless, this may explain the cognitive impairments commonly observed in advanced PD patients (Aarsland et al. 2001; Hobson and Meara 2004; Williams-Gray et al. 2009). Complementarily, excepting the correlation between motor impairment from left side and deep white matter of right frontal lobe (will be mentioned below), no significant laterization correlation was observed in our PD patients. We argued that lateralized neuronal degeneration is the hallmark for PD and is more significantly correlated with disease progression than white matter alterations (Martin et al. 2008), which probably explains the unparallel progression between lateralized white matter alterations and disease progression.

Moreover, we observed a decrease in MMS and RD in the left cerebellar hemisphere and a decrease in MMS in the bilateral deep white matter of the frontal lobes, of PD patients. A decrease in MMS and RD indicate an increase in diamagnetic tissues and an increased barrier to water diffusion in the radial direction, respectively. In the white matter of the left cerebellar hemisphere, myelin content provides the main source of changes in regional susceptibility and radial water diffusion (Song et al. 2002; Liu et al. 2011, 2015; Li et al. 2012; Lodygensky et al. 2012). Thus, our findings suggest an increase in myelination in this region, potentially reflecting enhanced structural connectivity between the cerebellum and cerebrum to improve cerebellar function in PD (Yu et al. 2007; Sen et al. 2010). Conversely, in the bilateral deep white matter of the frontal lobes, we found no corresponding change in DTI, likely because of the complexity of white matter directions within a single voxel in these regions (Tuch et al. 2002; Jeurissen et al. 2013). Interestingly, MMS in this region was negatively weakly correlated with contralateral motor impairment, disease duration and UPDRS II score. Exploratory trials suggested that UPDRS II was the most informative for determining baseline disease severity and subsequent disease progression in PD (Harrison et al. 2009; Parashos et al. 2014). These data suggest a partial increase in myelination in the frontal white matter potentially to compensate for overall cerebral dysfunction in PD, which demonstrated QSM provided more information than DTI.

PD patients suffering from motor impairment are classified as Braak pathologic stage 3 or 4 when the substantia nigra is involved (Braak et al. 2003, 2004). Lewy neurites and Lewy bodies infiltrate in an ascending course in the brain, involving the temporal, frontal, and parietal lobes (Braak et al. 2003, 2004). Degenerative alterations in white matter is considered to occur in PD progression. In

support, using QSM we found underlying pathologic alterations in the white matter adjacent to the temporal, frontal, and parietal regions. As PD patients diagnosed with clinical motor impairment are at moderate to advanced stages of disease, QSM may be a sensitive imaging biomarker for detecting underlying brain pathology, and to examine PD progression and evaluate disease status.

There were several limitations in the present study. First, it has been well known that the magnetic susceptibility in white matter has its anisotropy (STI or COSMOS) similar to the FA when using DTI (Liu 2010; Li et al. 2012; Liu et al. 2009, 2012; Li and Liu 2013). However, in the present study, we calculated MMS rather than susceptibility anisotropy. To minimize the influence of brain orientation with respect to the main magnetic field, we calculated the HRA relative to the B0 field, and used this as a main covariate during voxel-based statistics and correlation analyses. In current clinical practice, STI or COSMOS have the disadvantage of increased scanning time, and are also dependent on the ability to rotate patients' heads between scans, which limits their application. Second, 36 patients were accepting levodopa treatment. Therefore, its long-term effects might be inevitable which would potentially influence UPDRS scores, though all those patients were asked to terminated anti-parkinsonian medication for at least 12 h. Third, PD patients were examined at "off" medication. Thus, there was a relatively low number of diffusion directions acquired with the DTI data for the time constraints, which probably had a potential influence on the results. Fourth, although numerous studies, including our own, have reported white matter involvement in PD, there is limited pathologic confirmation in human brain tissue. Thus, further studies in PD animal models are required to assess the underlying pathologic changes in the brain related to QSM findings. Finally, susceptibility induced distortion in the DTI may, to some extent, influence the results in regions with large susceptibility gradients (e.g. frontal lobe, temporal lobe). To further validate the usefulness of QSM in white matter assessment, this problem should be solved in the future as a recently published study (Langley et al. 2016).

In conclusion, our data suggest that QSM may be a novel approach for detecting alterations in the white matter and examining the underlying network disruption in PD. Further, combination of QSM with DTI provides a more complete evaluation of the diseased brain by analyzing different biological tissue properties.

Acknowledgements We wish to thank all the participants including patients with Parkinson's disease and normal volunteers. We also thank the assistance from department of Neurology in our institute. Finally, Xiaojun Guan would like to personally thank Dr. Jingrui Jin, for her infinite patience, care and love.

Funding This work was supported by the 13th Five-year Plan for National Key Research and Development Program of China (Grant No. 2016YFC1306600), the Fundamental Research Funds for the Central Universities of China (2017XZZX001-01), the 12th Five-year Plan for National Science and Technology Supporting Program of China (Grant No. 2012BAI10B04) and the National Natural Science Foundation of China (Grant Nos. 81571654, 81371519, 81701647 and 81771820). P.H. was supported in part by the Projects of Medical and Health Technology Development Program in Zhejiang Province (2015KYB174) and C.L. was supported in part by the National Institutes of Health through grants NIMH R01MH096979, and by the National Natural Science Foundation of China (Grant No. 81428013).

Compliance with Ethical Standards

Conflict of interest The authors declare that they have no conflict of interest.

Informed Consent Informed consent was obtained from all individual participants included in the study.

Ethical approval All procedures performed in study involving human participants were in accordance with the ethical standards of the institutional and/or national research committee and with the 1964 Helsinki declaation and its later amendments or comparable ethical standards.

References

Aarsland, D., Andersen, K., Larsen, J. P., Lolk, A., Nielsen, H., & Kragh-Sorensen, P. (2001). Risk of dementia in Parkinson's disease: a community-based, prospective study. *Neurology, 56*, 730–736.

Agosta, F., Canu, E., Stefanova, E., Sarro, L., Tomic, A., Spica, V., Comi, G., Kostic, V. S., & Filippi, M. (2014). Mild cognitive impairment in Parkinson's disease is associated with a distributed pattern of brain white matter damage. *Human Brain Mapping, 35*, 1921–1929.

Agosta, F., Canu, E., Stojkovic, T., Pievani, M., Tomic, A., Sarro, L., Dragasevic, N., Copetti, M., Comi, G., Kostic, V. S., & Filippi, M. (2013). The topography of brain damage at different stages of Parkinson's disease. *Human Brain Mapping, 34*, 2798–2807.

Argyridis, I., Li, W., Johnson, G. A., & Liu, C. (2013). Quantitative magnetic susceptibility of the developing mouse brain reveals microstructural changes in the white matter. *Neuroimage, 88C*, 134–142.

Auning, E., Kjaervik, V. K., Selnes, P., Aarsland, D., Haram, A., Bjornerud, A., Hessen, E., Esnaashari, A., & Fladby, T. (2014). White matter integrity and cognition in Parkinson's disease: a cross-sectional study. *British Medical Journal Open, 4*, e3976.

Beaulieu, C. (2002). The basis of anisotropic water diffusion in the nervous system - a technical review. *NMR Biomedicine, 15*, 435–455.

Braak, H., Del, T. K., Rub, U., de Vos, R. A., Jansen, S. E., & Braak, E. (2003). Staging of brain pathology related to sporadic Parkinson's disease. *Neurobiology of Aging, 24*, 197–211.

Braak, H., Ghebremedhin, E., Rub, U., Bratzke, H., & Del, T. K. (2004). Stages in the development of Parkinson's disease-related pathology. *Cell and Tissue Research, 318*, 121–134.

Chen, B., Fan, G. G., Liu, H., & Wang, S. (2015). Changes in anatomical and functional connectivity of Parkinson's disease patients according to cognitive status. *European Journal of Radiology, 84*, 1318–1324.

Delano-Wood, L., Stricker, N. H., Sorg, S. F., Nation, D. A., Jak, A. J., Woods, S. P., Libon, D. J., Delis, D. C., Frank, L. R., & Bondi, M. W. (2012). Posterior cingulum white matter disruption and its associations with verbal memory and stroke risk in mild cognitive impairment. *Journal of Alzheimers Disease, 29*, 589–603.

Du, G., Liu, T., Lewis, M. M., Kong, L., Wang, Y., Connor, J., Mailman, R. B., & Huang, X. (2015) Quantitative susceptibility mapping of the midbrain in Parkinson's disease. Movement Disorders.

Fazekas, F., Chawluk, J. B., Alavi, A., Hurtig, H. I., & Zimmerman, R. A. (1987). MR signal abnormalities at 1.5 T in Alzheimer's dementia and normal aging. *AJR American Journal of Roentgenology, 149*, 351–356.

Gallagher, C., Bell, B., Bendlin, B., Palotti, M., Okonkwo, O., Sodhi, A., Wong, R., Buyan-Dent, L., Johnson, S., Willette, A., Harding, S., Ninman, N., Kastman, E., & Alexander, A. (2013). White matter microstructural integrity and executive function in Parkinson's disease. *Journal of the International Neuropsychological Society, 19*, 349–354.

Gattellaro, G., Minati, L., Grisoli, M., Mariani, C., Carella, F., Osio, M., Ciceri, E., Albanese, A., & Bruzzone, M. G. (2009). White matter involvement in idiopathic Parkinson disease: a diffusion tensor imaging study. *AJNR American Journal of Neuroradiology, 30*, 1222–1226.

Guan, X., Xuan, M., Gu, Q., Huang, P., Liu, C., Wang, N., Xu, X., Luo, W., & Zhang, M. (2017a) Regionally progressive accumulation of iron in Parkinson's disease as measured by quantitative susceptibility mapping. *NMR in Biomedicine, 30*(4). https://doi.org/10.1002/nbm.3489.

Guan, X., Xuan, M., Gu, Q., Xu, X., Huang, P., Wang, N., Shen, Z., Xu, J., Luo, W., & Zhang, M. (2017b). Influence of regional iron on the motor impairments of Parkinson's disease: A quantitative susceptibility mapping study. *Journal of Magnetic Resonance Imaging, 45*, 1335–1342.

Harrison, M. B., Wylie, S. A., Frysinger, R. C., Patrie, J. T., Huss, D. S., Currie, L. J., & Wooten, G. F. (2009). UPDRS activity of daily living score as a marker of Parkinson's disease progression. *Movement Disorders, 24*, 224–230.

He, N., Ling, H., Ding, B., Huang, J., Zhang, Y., Zhang, Z., Liu, C., Chen, K., & Yan, F. (2015). Region-specific disturbed iron distribution in early idiopathic Parkinson's disease measured by quantitative susceptibility mapping. *Human Brain Mapping, 36*, 4407–4420.

Hobson, P., & Meara, J. (2004). Risk and incidence of dementia in a cohort of older subjects with Parkinson's disease in the United Kingdom. *Movement Disorders, 19*, 1043–1049.

Hughes, A. J., Daniel, S. E., Kilford, L., & Lees, A. J. (1992). Accuracy of clinical diagnosis of idiopathic Parkinson's disease: a clinico-pathological study of 100 cases. *Journal of Neurology Neurosurgery, and Psychiatry, 55*, 181–184.

Jeurissen, B., Leemans, A., Tournier, J. D., Jones, D. K., & Sijbers, J. (2013). Investigating the prevalence of complex fiber configurations in white matter tissue with diffusion magnetic resonance imaging. *Human Brain Mapping, 34*, 2747–2766.

Jones, D. K., Knosche, T. R., & Turner, R. (2013). White matter integrity, fiber count, and other fallacies: the do's and don'ts of diffusion MRI. *Neuroimage, 73*, 239–254.

Kamagata, K., Motoi, Y., Tomiyama, H., Abe, O., Ito, K., Shimoji, K., Suzuki, M., Hori, M., Nakanishi, A., Sano, T., Kuwatsuru, R., Sasai, K., Aoki, S., & Hattori, N. (2013). Relationship between cognitive impairment and white-matter alteration in Parkinson's disease with dementia: tract-based spatial statistics and tract-specific analysis. *European Radiology, 23*, 1946–1955.

Karagulle, K. A., Lehericy, S., Luciana, M., Ugurbil, K., & Tuite, P. (2008). Altered diffusion in the frontal lobe in Parkinson disease. *AJNR American Journal of Neuroradiology, 29*, 501–505.

Katzman, R., Zhang, M. Y., Ouang-Ya Qu, Wang, Z. Y., Liu, W. T., Yu, E., Wong, S. C., Salmon, D. P., & Grant, I. (1988). A Chinese version of the Mini-Mental State Examination; impact of illiteracy in a Shanghai dementia survey. *Journal of Clinical Epidemiology, 41*, 971–978.

Langley, J., Huddleston, D. E., Merritt, M., Chen, X., McMurray, R., Silver, M., Factor, S. A., & Hu, X. (2016). Diffusion tensor imaging of the substantia nigra in Parkinson's disease revisited. *Human Brain Mapping, 37*, 2547–2556.

Lee, J., Shmueli, K., Fukunaga, M., van Gelderen, P., Merkle, H., Silva, A. C., & Duyn, J. H. (2010) Sensitivity of MRI resonance frequency to the orientation of brain tissue microstructure. Proceeding of the National Academy of Science of the United States of America 107: 5130–5135.

Li, W., & Liu, C. (2013). Comparison of Magnetic Susceptibility Tensor and Diffusion Tensor of the Brain. *Journal of Neuroscience and Neuroengineer, 2*, 431–440.

Li, W., Wang, N., Yu, F., Han, H., Cao, W., Romero, R., Tantiwongkosi, B., Duong, T. Q., & Liu, C. (2015). A method for estimating and removing streaking artifacts in quantitative susceptibility mapping. *Neuroimage, 108*, 111–122.

Li, W., Wu, B., Avram, A. V., & Liu, C. (2012). Magnetic susceptibility anisotropy of human brain in vivo and its molecular underpinnings. *Neuroimage, 59*, 2088–2097.

Li, W., Wu, B., Batrachenko, A., Bancroft-Wu, V., Morey, R. A., Shashi, V., Langkammer, C., De Bellis, M. D., Ropele, S., Song, A. W., & Liu, C. (2014). Differential developmental trajectories of magnetic susceptibility in human brain gray and white matter over the lifespan. *Human Brain Mapping, 35*, 2698–2713.

Li, W., Wu, B., & Liu, C. (2011). Quantitative susceptibility mapping of human brain reflects spatial variation in tissue composition. *Neuroimage, 55*, 1645–1656.

Li, X., Vikram, D. S., Lim, I. A., Jones, C. K., Farrell, J. A., & van Zijl, P. C. (2012). Mapping magnetic susceptibility anisotropies of white matter in vivo in the human brain at 7 T. *Neuroimage, 62*, 314–330.

Liu, C. (2010). Susceptibility tensor imaging. *Magn Reson Med, 63*, 1471–1477.

Liu, T., Spincemaille, P., de Rochefort, L., Kressler, B., & Wang, Y. (2009). Calculation of susceptibility through multiple orientation sampling (COSMOS): a method for conditioning the inverse problem from measured magnetic field map to susceptibility source image in MRI. *Magnetic Resonance in Medicine, 61*(1), 196–204.

Liu, C., Li, W., Johnson, G. A., & Wu, B. (2011). High-field (9.4 T) MRI of brain dysmyelination by quantitative mapping of magnetic susceptibility. *Neuroimage, 56*, 930–938.

Liu, C., Li, W., Wu, B., Jiang, Y., & Johnson, G. A. (2012). 3D fiber tractography with susceptibility tensor imaging. *Neuroimage, 59*, 1290–1298.

Liu, C., Li, W., Tong, K. A., Yeom, K. W., & Kuzminski, S. (2015). Susceptibility-weighted imaging and quantitative susceptibility mapping in the brain. *Journal of Magnetic Resonance Imaging, 42*, 23–41.

Lodygensky, G. A., Marques, J. P., Maddage, R., Perroud, E., Sizonenko, S. V., Huppi, P. S., & Gruetter, R. (2012). In vivo assessment of myelination by phase imaging at high magnetic field. *Neuroimage, 59*, 1979–1987.

Martin, W. R., Wieler, M., & Gee, M. (2008). Midbrain iron content in early Parkinson disease: a potential biomarker of disease status. *Neurology, 70*, 1411–1417.

Murakami, Y., Kakeda, S., Watanabe, K., Ueda, I., Ogasawara, A., Moriya, J., Ide, S., Futatsuya, K., Sato, T., Okada, K., Uozumi, T., Tsuji, S., Liu, T., Wang, Y., & Korogi, Y. (2015) Usefulness of Quantitative Susceptibility Mapping for the Diagnosis of Parkinson Disease. In, Vol. 36, pp. 1102–1108.

Neil, J., Miller, J., Mukherjee, P., & Huppi, P. S. (2002). Diffusion tensor imaging of normal and injured developing human brain - a technical review. *NMR Biomedicine, 15*, 543–552.

Parashos, S. A., Luo, S., Biglan, K. M., Bodis-Wollner, I., He, B., Liang, G. S., Ross, G. W., Tilley, B. C., & Shulman, L. M. (2014). Measuring disease progression in early Parkinson disease: the National Institutes of Health Exploratory Trials in Parkinson Disease (NET-PD) experience. *JAMA Neurology, 71*, 710–716.

Rae, C. L., Correia, M. M., Altena, E., Hughes, L. E., Barker, R. A., & Rowe, J. B. (2012). White matter pathology in Parkinson's disease: the effect of imaging protocol differences and relevance to executive function. *Neuroimage, 62*, 1675–1684.

Rudko, D. A., Solovey, I., Gati, J. S., Kremenchutzky, M., & Menon, R. S. (2014). Multiple sclerosis: improved identification of disease-relevant changes in gray and white matter by using susceptibility-based MR imaging. *Radiology, 272*, 851–864.

Sen, S., Kawaguchi, A., Truong, Y., Lewis, M. M., & Huang, X. (2010). Dynamic changes in cerebello-thalamo-cortical motor circuitry during progression of Parkinson's disease. *Neuroscience, 166*, 712–719.

Song, S. K., Sun, S. W., Ramsbottom, M. J., Chang, C., Russell, J., & Cross, A. H. (2002). Dysmyelination revealed through MRI as increased radial (but unchanged axial) diffusion of water. *Neuroimage, 17*, 1429–1436.

Surdhar, I., Gee, M., Bouchard, T., Coupland, N., Malykhin, N., & Camicioli, R. (2012). Intact limbic-prefrontal connections and reduced amygdala volumes in Parkinson's disease with mild depressive symptoms. *Parkinsonism & Related Disorders, 18*, 809–813.

Tuch, D. S., Reese, T. G., Wiegell, M. R., Makris, N., Belliveau, J. W., & Wedeen, V. J. (2002). High angular resolution diffusion imaging reveals intravoxel white matter fiber heterogeneity. *Magnetic Resonance in Medicine, 48*, 577–582.

Williams-Gray, C. H., Evans, J. R., Goris, A., Foltynie, T., Ban, M., Robbins, T. W., Brayne, C., Kolachana, B. S., Weinberger, D. R., Sawcer, S. J., & Barker, R. A. (2009). The distinct cognitive syndromes of Parkinson's disease: 5 year follow-up of the CamPaIGN cohort. *Brain, 132*, 2958–2969.

Worker, A., Blain, C., Jarosz, J., Chaudhuri, K. R., Barker, G. J., Williams, S. C., Brown, R. G., Leigh, P. N., Dell'Acqua, F., & Simmons, A. (2014). Diffusion tensor imaging of Parkinson's disease, multiple system atrophy and progressive supranuclear palsy: a tract-based spatial statistics study. *PLoS One, 9*, e112638.

Wu, B., Li, W., Guidon, A., & Liu, C. (2012). Whole brain susceptibility mapping using compressed sensing. *Magnetic Resonance in Medicine, 67*, 137–147.

Yu, H., Sternad, D., Corcos, D. M., & Vaillancourt, D. E. (2007). Role of hyperactive cerebellum and motor cortex in Parkinson's disease. *Neuroimage, 35*, 222–233.

Zhan, W., Kang, G. A., Glass, G. A., Zhang, Y., Shirley, C., Millin, R., Possin, K. L., Nezamzadeh, M., Weiner, M. W., Marks, W. J., & Schuff, N. (2012). Regional alterations of brain microstructure in Parkinson's disease using diffusion tensor imaging. *Movement Disorders, 27*, 90–97.

Zhang, M. Y., Katzman, R., Salmon, D., Jin, H., Cai, G. J., Wang, Z. Y., Qu, G. Y., Grant, I., Yu, E., Levy, P., & Et, A. (1990). The prevalence of dementia and Alzheimer's disease in Shanghai, China: impact of age, gender, and education. *Annals of Neurology, 27*, 428–437.